35

Flows Involving Phase Change

Herbert E. Huppert
University of Cambridge

M. Grae Worster
University of Cambridge

35.1 Introduction

Flows involving phase change are ubiquitous in geophysical and industrial settings and are vital for life on Earth. For example, the solid iron inner core of the Earth solidifies from the molten outer core and releases buoyant constituents that drive compositional convection and power the geo-dynamo that generates our magnetic field. Melting and re-solidification of silicates in the mantle and crust generate new rocks and segregate economically important minerals into mineable seams. Groundwater is converted to steam in geothermal reservoirs that can be tapped for energy production. The oceans freeze and thaw in annual cycles, moderating global temperatures and driving ocean circulations. Surface waters evaporate, rise, and re-condense to form clouds and life-giving rain. And from the Bronze Age onward, melting and solidification have been central to many technological developments.

In this chapter, we introduce the key thermodynamic and fluid-mechanical principles that govern phase changes, explaining how flow in fluid melts can both be driven by and influence those changes. Our discussions are illustrated mostly by geophysical examples, particularly phenomena occurring in our oceans and atmosphere but also some that occur in water-saturated soils, in magmatic systems, and in industrial processes.

35.2 Principles

Changes of phase, from liquid water to vapor or to solid ice, for example, are thermodynamic processes requiring the transport of heat and sometimes, as in the case of freezing salt water, of a chemical component. Therefore, flows involving phase change are inevitably associated with temperature gradients and possibly also compositional gradients. Both can cause density gradients and associated buoyancy forces. The importance of phase change to a given flow can be assessed by estimating certain key dimensionless parameters.

35.2.1 Thermodynamic Considerations

We can distinguish two important situations: those in which phase change occurs at the boundary of a fluid domain or at the interface between fluid domains and those in which phase change occurs in the interior of a fluid domain. Examples of the former are the melting of an iceberg and the evaporation of a pool of water. Examples of the latter are condensation in the interiors of clouds and dissolution in the interior of sea ice.

When phase change occurs at a boundary, a key dimensionless parameter is the Stefan number

$$\mathcal{S} = \frac{L}{c_p \Delta T},$$

where

- L is the latent heat per unit mass associated with change of phase at constant temperature
- c_p is the specific heat capacity of the medium through which the latent heat is principally transported in order to effect the phase change
- ΔT is the characteristic temperature difference driving that heat transport

Handbook of Environmental Fluid Dynamics, Volume One, edited by Harindra Joseph Shermal Fernando. © 2013 CRC Press/Taylor & Francis Group, LLC. ISBN: 978-1-4398-1669-1.

When the Stefan number is large, the motion of the phase boundary is slow compared to the rate of thermal processes in the media on either side, whether or not the media are flowing. To a good approximation, therefore, the heat transfer rates and any fluid flow can be calculated assuming that the phase boundary is stationary, and the evolution of the phase boundary can be determined subsequently.

In the transition from ice to water, L/c_p is about 80°C in the water and about 160°C in the ice, while in the transition from liquid water to water vapor, L/c_p is about 600°C in the water and about 2500°C in the vapor. In all these cases and for geophysically relevant flows, for which ΔT is typically only a few degrees Celsius, the Stefan number is therefore indeed large and the quasi-stationary approximation can be used with confidence.

Regions of mixed phase can exist when there are variations of two (or more) thermodynamic variables that determine the state of the matter. A well known and geophysically important example occurs during the freezing of salt water. The equilibrium (liquidus) temperature T_L between ice and salt water decreases with the salinity S of the latter. In many circumstances, this relationship can be approximated linearly by

$$T_L(S) = T_0 - m(S - S_0),$$

where

S_0 is a reference value of the salinity at which $T_L = T_0$
m is the slope of the liquidus

For seawater $m \approx 0.05$°C psu^{-1}, where the practical salinity unit (psu), defined in terms of conductivity, corresponds closely to parts per thousand of sodium chloride.

Another important thermodynamic variable in geophysical contexts is pressure, which influences the equilibrium freezing temperature $T_e(p)$ according to the Clausius–Clapeyron relationship

$$L\frac{T_m - T_e(p)}{T_m} = (p - p_m)\left(\frac{1}{\rho_s} - \frac{1}{\rho_l}\right),$$

where

T_m is the freezing temperature at pressure p_m
ρ_s and ρ_l are the densities of the solid and liquid phases, respectively

Therefore, the inner core of the Earth, which is virtually pure iron with $\rho_s > \rho_l$, is solid owing to the high pressures there, even though it is hotter than the outer core of molten iron. On the other hand, because the density of ice is less than that of water, marine ice sheets in Antarctica melt at their basal contact with the deep ocean, even though the temperature there is about –2°C.

Pressure is continuous across a planar interface between bulk phases in equilibrium. But if there is a pressure difference between a solid and its liquid melt, either because surface tension acts across a curved interface between them or because disjoining forces act in proximity to a substrate, then the equilibrium freezing temperature T_e is depressed according to

$$\rho_s L\frac{T_m - T_e}{T_m} = p_s - p_l.$$

In the case of a curved interface with surface tension γ_{sl} and principal radius of curvature R, this gives the Gibbs–Thomson relationship

$$\rho_s L\frac{T_m - T_e}{T_m} = \frac{\gamma_{sl}}{R},$$

which stabilizes morphological instabilities of phase boundaries (see later) and hence influences the scale and patterns of snowflakes, for example.

When a mixture, like salt water, begins to freeze, one of the components is preferentially incorporated into the solid phase, while the remaining liquid is enriched in the other. At low salinities, typical of the ocean, the solid phase is almost pure ice, and salt is rejected as sea ice forms. The rate of phase change at a planar interface is governed by the rate of removal of excess salt, rather than by the rate of removal of latent heat. The important dimensionless parameter is the concentration ratio

$$\mathcal{C} = \frac{(S_0 - S_s)}{\Delta S},$$

where

S_s is the salinity of the solid phase (equal to zero in the case of ice formed from salt water)
ΔS is the characteristic salinity difference driving salt transport in the liquid phase

Usually the solid–liquid interface is close to equilibrium and

$$\Delta S = \frac{(T_0 - T_i)}{m},$$

where T_i is the temperature of the interface.

In consequence of the fact that salt diffuses slower than heat, a phenomenon called constitutional supercooling usually occurs in the liquid adjacent to the phase boundary during solidification of a mixture. This is the phenomenon of having liquid at a temperature below its freezing (liquidus) temperature in consequence of locally altered salinity. It is relieved in most natural and many industrial settings by a morphological instability of the phase boundary that results in the formation of a mushy layer: a region of mixed phase comprising small-scale, often dendritic, solid crystals bathed in residual melt. Mushy layers are reactive porous media (Worster 2000) whose porosity and permeability can change in response to changes in temperature and salinity caused by advection and diffusion.

Latent heat is released in the interior of a mushy layer during solidification as the volume fraction of solid crystals increases. The effective specific heat capacity (the heat energy required to raise or lower the temperature by 1°) of a mushy layer is thereby augmented by a factor characterized by the dimensionless group

$$\Omega = 1 + \frac{\mathcal{S}}{\mathcal{C}} = 1 + \frac{L}{c_p m(S_0 - S_s)}.$$

If there is a larger salinity difference between solid and liquid phases, then the change in solid fraction associated with a given change in temperature is smaller, and hence the internal release of latent heat is inversely related to $\mathcal{C}$. A similar effect occurs in moist convection, where the effective heat capacity is equal to the heat capacity of dry air augmented by a factor approximately equal to

$$\Omega = 1 + \frac{L^2 q}{c_p \mathcal{R} T^2}$$

(Stevens 2005), where

q is the mass fraction of water vapor
$\mathcal{R}$ is the gas constant

The analogy is clear once we associate q with S, the saturation of the condensed phase $q_s = 1 \gg q$ with S_s and the liquidus slope m with $-\partial T/\partial q \approx -\mathcal{R}T^2/Lq$.

35.2.2 Buoyancy-Driven Convection

These sorts of considerations have a profound influence on the buoyancy forcing of the oceans and clouds. The density of salt water, for example, varies approximately linearly as

$$\rho = \rho_0\left[1 - \alpha(T - T_0) + \beta(S - S_0)\right],$$

for small temperature and salinity variations, where ρ_0 is the reference density when $(T, S) = (T_0, S_0)$ and α and β are the coefficients of thermal expansion and solutal density variation, respectively. Pure water attains a maximum density at 4°C, at which temperature $\alpha = 0$. The temperature at which salt water attains its maximum density decreases as salinity increases until, for S greater than about 14 psu, there is no density maximum and α is positive for all temperatures above the liquidus. However, α remains very sensitive to temperature at temperatures close to the liquidus, and seawater, whose salinity is around 30–35 psu, has a value of $\alpha \approx 10^{-5}$ near its liquidus temperature of about −2°C (typical of polar conditions), compared with a value of $\alpha \approx 10^{-4}$ at 20°C.

In a *polynya*, growing ice crystals are blown down wind and the open ocean is continuously exposed to the cold atmosphere. A heat flux F from ocean to atmosphere creates ice crystals, which increases the salinity of the remaining liquid and causes a buoyancy flux

$$F_{BS} = \rho_0 g\beta \frac{\partial S}{\partial t} = \rho_0 g\beta S_0 \frac{\partial \phi}{\partial t} = \rho_0 g\beta S_0 \frac{F}{\rho_s L},$$

where

S and ϕ are the salinity and solid fraction in a parcel of freezing ocean of unit volume
g is the acceleration due to gravity

This can be contrasted with the buoyancy flux

$$F_{BT} = -\rho_0 g\alpha \frac{\partial T}{\partial t} = \frac{g\alpha F}{c_p}$$

that results from cooling the ocean without freezing. The ratio of these buoyancy fluxes

$$\frac{F_{BS}}{F_{BT}} = \frac{\rho_0}{\rho_s} \frac{\beta S_0}{\alpha} \frac{c_p}{L}$$

is about 20 in the polar oceans, which is why the densest abyssal waters are generated around Antarctica, where polynyas are commonly formed by strong katabatic winds off the continent, and, to a lesser extent, in the Greenland Sea. In contrast, where sea ice becomes consolidated, typical of the Arctic Ocean, it insulates the ocean from atmospheric cooling, and brine production is much weaker.

A similar expression relates the buoyancy fluxes associated with salinity increase and cooling resulting from evaporation in warmer waters, such as the Mediterranean. However, because α is significantly larger at those temperatures and salinities, and the latent heat of vaporization is much larger than that of freezing, the balance is reversed: cooling is then more potent than salinity increase at producing buoyancy fluxes by a factor of about 4 (Gill 1982).

Buoyancy forces can cause convection in a fluid (Turner 1979), which can have profound effects on phase changes in the fluid. Whether or not convection occurs and the strength and character of any convection when it does occur are determined by the magnitude of the Rayleigh number. This dimensionless number characterizes the potential energy of the fluid due to buoyancy relative to the dissipation of buoyancy by diffusion and of energy by viscosity as the system attempts to convert its potential energy into the kinetic energy of fluid motion.

In a fluid whose density is affected only by temperature, the Rayleigh number is

$$Ra_T = \frac{\alpha \Delta T g h^3}{\kappa \nu},$$

where

h is a characteristic vertical length scale for the fluid system
κ and ν are the thermal diffusivity and kinematic viscosity of the fluid, respectively

This reflects the fact that the buoyancy is due to temperature gradients and is dissipated by thermal diffusion. By direct analogy, if the density is affected only by salinity, then the appropriate Rayleigh number is

$$Ra_S = \frac{\beta \Delta S g h^3}{D\nu},$$

where D is the diffusivity of salt in water. In fluids whose density is simultaneously affected by thermal and salinity variations, both Rayleigh numbers are important. Indeed, fascinating forms of convection, so-called double-diffusive convection, can occur even when the overall density of fluid decreases with height, so that the system is apparently stably stratified, provided that there is potential energy associated with either the temperature or the salinity field (Huppert and Turner 1981). Such flows owe their existence to the fact that heat and salt diffuse at different rates, which allows the potential energy of the unstably stratified component to be exploited. A ubiquitous feature of double-diffusive convection is the spontaneous development of discrete layers of fluid motion, illustrated in Figure 35.6. It has been suggested that such fluid-mechanical layering during solidification can result in layered structures within igneous intrusions, for example.

There are many interesting and important geophysical flows involving phase change that take place in porous media. Examples include natural hydrothermal flow of groundwater and the flow of supercritical carbon dioxide in aquifers during attempts at sequestering unwanted CO_2 from gas and oil fields and other industrial sources. In a porous medium, the relevant thermal Rayleigh number is

$$Ra_p = \frac{\alpha \Delta T g h \Pi}{\kappa \nu},$$

where Π is the permeability of the medium. This reflects the fact that viscous dissipation occurs on the scale of the pores of the medium, which is proportional to $\sqrt{\Pi}$.

A fascinating hybrid of these results occurs in a mushy layer. The temperature and interstitial salinity of a mushy layer are coupled by the liquidus relationship, so the density variation is given by

$$\rho = \rho_0 \left[1 + \left(\frac{(\beta - \alpha)}{m} \right) (S - S_0) \right]$$

and there is no propensity for double-diffusive convection. Typically $\beta \gg \alpha/m$, and the characteristic Rayleigh number is

$$Ra_m = \frac{\beta \Delta S g h \Pi}{\kappa \nu}.$$

This reflects the facts that a mushy layer acts as a porous medium, that the buoyancy is dominated by salinity variations, but that the dissipation of buoyancy results from internal phase change, mediated by the thermal field altering the interstitial salinity (Worster 2000). As described earlier, the internal release of latent heat augments the effective heat capacity of the mushy layer, so the effective thermal diffusivity is κ/Ω and, as we shall see later, the critical parameter for convection in a mushy layer is therefore ΩRa_m.

In this section, we have introduced many of the dimensionless parameters governing flows involving phase change. They will appear and be illustrated further as we explore specific examples later.

35.3 Methods of Analysis

Our understanding of flows involving phase change has benefited enormously from studies that have combined laboratory experimentation with theoretical and computational developments. Here we outline some of the most common approaches, starting again with single-component systems.

35.3.1 Scaling and Similarity Solutions

Significant physical insight and understanding can be gained from scaling analyses, which in some important circumstances can lead to similarity solutions. This is the case in what has become known as Neumann's solution to the Stefan problem, though Neumann's analysis seems to predate Stefan's own investigation! In the simplest version, depicted in Figure 35.1 and described in Carslaw and Jaeger (1959) for example, a deep layer of liquid (ocean) at its freezing temperature T_m has its fixed boundary maintained at a constant lower temperature T_0. Solid (ice) forms a layer of thickness $h(t)$ adjacent to the cooled boundary. The temperature $T(z, t)$ in the solid satisfies the diffusion equation

$$T_t = kT_{zz} \quad (0 < z < h(t))$$

and conservation of heat at the solid–liquid interface is expressed by the Stefan condition

$$\rho L \dot{h} = \kappa T_z \big|_{z=h},$$

where $k = \rho c_p \kappa$ is the thermal conductivity. Since there is no externally imposed nor any intrinsic length scale in the problem, there is a similarity solution with

$$T(z,t) = T_0 + (T_m - T_0)\,\mathrm{erf}\left(\frac{z}{2\sqrt{\kappa t}} \right) \quad \text{and} \quad h(t) = 2\lambda\sqrt{\kappa t}.$$

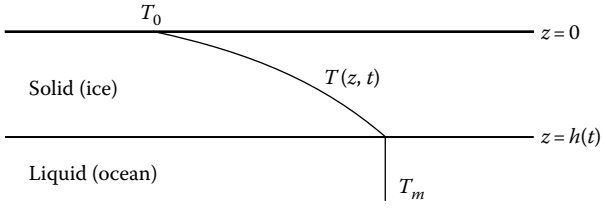

FIGURE 35.1 A simple Stefan problem, in which solid forms at the cooled boundary of a deep layer of melt at its freezing temperature.

The growth parameter λ is determined by the transcendental equation

$$\sqrt{\pi}\lambda e^{\lambda^2}\ \mathrm{erf}\lambda = \mathcal{S}^{-1},$$

where $\mathcal{S} = L/c_p(T_m - T_0)$.

A useful and instructive approximation can be found when $\mathcal{S}$ is large, in which case the temperature field is quasi-steady and therefore linear. The Stefan condition then has the simple form

$$\rho L\dot{h} = \frac{k(T_m - T_0)}{h},$$

which is readily integrated to give

$$h = \sqrt{\frac{2\kappa t}{\mathcal{S}}}.$$

A comparison between this approximate result and the exact solution is shown in Figure 35.2a.

Many important analytical and computational methods have been developed in terms of the enthalpy of the system. A new and revealing example of such an approach is provided by the case of a solid at temperature T_m growing into a supercooled liquid of temperature $T_\infty < T_m$, as depicted in Figure 35.3. The total enthalpy of this system relative to the far field (at constant pressure) is

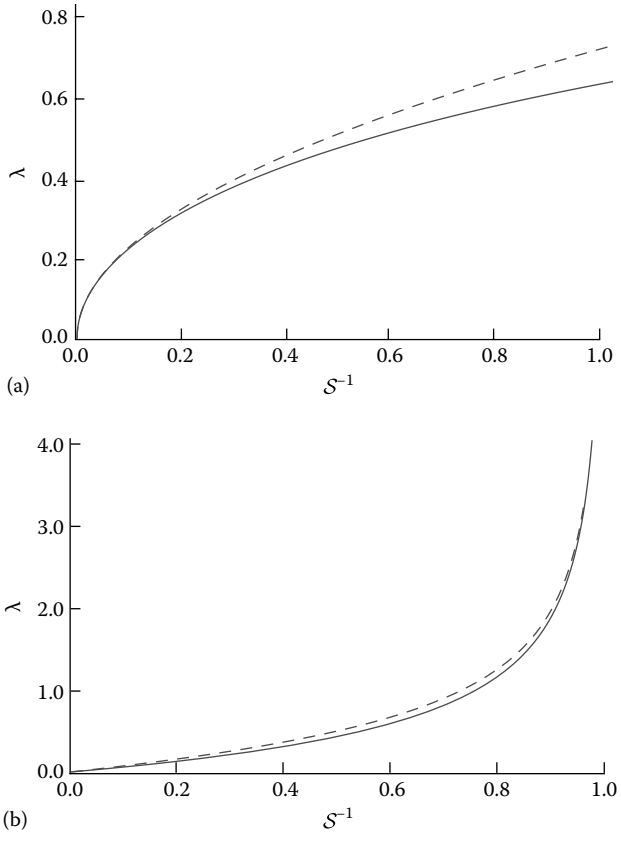

FIGURE 35.2 The growth parameter λ as a function of the inverse Stefan number $\mathcal{S}^{-1}$ for solidification at a cooled boundary (a) and into a supercooled melt (b). In the latter case, there is no solution for $S < 1$. The solid curves show the similarity solutions of the full diffusion equation. The dashed curves show the approximate solutions described in the text.

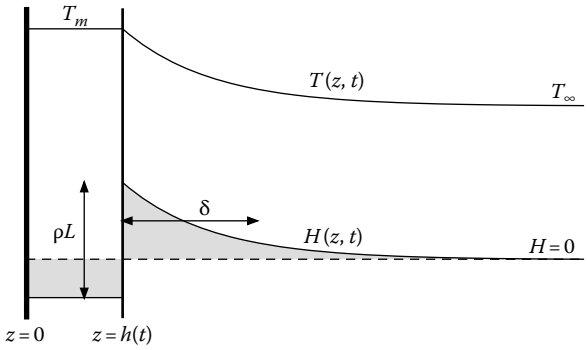

FIGURE 35.3 The temperature T and enthalpy H for a solid growing into a supercooled melt. Conservation of enthalpy means that the two shaded regions must have equal area, which cannot be achieved if the latent heat L is too small.

$$H = \left[-\rho L + \rho c_p(T_m - T_\infty)\right]h + \int_h^\infty \rho c_p(T - T_\infty)dz.$$

We can approximate the integral by $\rho c_p(T_m - T_\infty)\delta$, where δ is a scale length (boundary-layer thickness) for the temperature field, and use conservation of enthalpy, given the initial condition that $H = 0$, to deduce that $\delta = (\mathcal{S} - 1)h$, where $\mathcal{S} = L/c_p(T_m - T_\infty)$. In this case, the Stefan condition can be approximated by

$$\rho L\dot{h} = \frac{k(T_m - T_\infty)}{\delta},$$

whence

$$h = \sqrt{\frac{2\kappa t}{\mathcal{S}(\mathcal{S} - 1)}}.$$

This is compared with the exact similarity solution $h = 2\lambda\sqrt{\kappa t}$, with $\sqrt{\pi}\lambda e^{\lambda^2}\,\mathrm{erfc}\lambda = \mathcal{S}^{-1}$ in Figure 35.2b. The quantitative effectiveness of the approximation is of secondary importance to the insight that can be gained from the structure revealed by it. We see immediately that the predicted rate of solidification tends to infinity as $\mathcal{S} \to 1+$, and that there is no solution when $\mathcal{S} < 1$. The enthalpy formulation reveals the fact that the solid is predicted to have positive enthalpy when $\mathcal{S} < 1$, and that the total enthalpy cannot therefore be conserved. In this case, one must take account of the kinetics of molecular attachment and recognize on the continuum level that the solid–liquid interface is below the equilibrium freezing temperature T_m during solidification (Worster 2000).

The two previous approaches can be combined or the method of Neumann extended straightforwardly to consider the case of a melt initially at a temperature greater than T_m brought into contact with a boundary held at a temperature less than T_m. The additional diffusive heat transport from the liquid typically plays a minor role in comparison with the latent heat that must be removed through the solid phase to the boundary.

35.3.2 Perturbation Analysis

An important phenomenon that occurs when the liquid is supercooled is morphological instability: small corrugations of the solid–liquid interface grow into the branched patterns of snowflakes or Jack Frost, for example. The same phenomenon is common during solidification of a mixture, as depicted in Figure 35.4. In this illustrative example, we employ the frozen temperature approximation (Davis 2001) that the temperature field remains unperturbed with a uniform gradient G. In the liquid near the interface, the salt rejected during solidification creates a salinity gradient G_S. When the initially planar interface at $z = 0$ is perturbed to position

$$z = \eta(x,t) = \hat{\eta} A e^{i\alpha x + \sigma t},$$

there is a corresponding perturbation to the salinity field, which to good approximation satisfies Laplace's equation so that

$$S(x,z,t) = S_0 - G_S z + \Theta e^{-\alpha z} e^{i\alpha x + \sigma t}$$

where $\hat{\eta}$ and Θ are constants, while

$$T(x,z,t) = T_0 + Gz,$$

where we have chosen $(S, T) = (S_0, T_0)$ to correspond to the salinity and the corresponding liquidus temperature at the unperturbed interface.

The temperature of the curved interface

$$T(x,\eta,t) = -mS(x,\eta,t) - \Gamma(-\eta_{xx}) \quad (z = \eta)$$

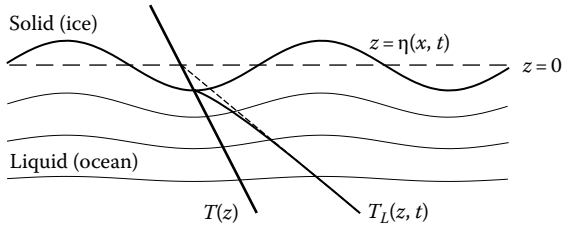

FIGURE 35.4 The thick sinusoidal curve shows the perturbed position $z = \eta(x, t)$ of the solid–liquid interface, originally at $z = 0$. The thinner sinusoidal curves show perturbed contours of concentration in the liquid: they are closer together near protrusions of the solid into the liquid, which enhances diffusion of solute away from the solidification front and promotes instability. The thick solid line shows the (frozen) temperature field. The thinner curve and short-dashed curve show the perturbed and original vertical salinity profiles, expressed as the local liquidus temperature.

is equal to the liquidus temperature depressed by an amount proportional to its curvature, with constant of proportionality Γ, according to the Gibbs–Thomson effect. Conservation of salt is expressed by

$$S\eta_t = -DS_x \quad (z = \eta),$$

which is similar in form to the Stefan condition.

By substituting the aforementioned expressions for the temperature and salinity fields into the two interfacial conditions and linearizing in the small perturbation quantities, we find the dispersion relation

$$\sigma = \frac{D}{mS_0}\alpha\left[(mG_S - G) - \Gamma\alpha^2\right]$$

for the growth rate σ of disturbances of wavenumber α.

In this simple, idealized model, we see that there are positive growth rates and disturbances will grow if $G < mG_S$, which corresponds to there being constitutional supercooling (temperatures less than the liquidus) of the unperturbed liquid.

35.3.3 Continuum Modeling of Mushy Layers

Once significant morphological instability has occurred and a mushy layer has formed, it is no longer practical to follow the evolution of the solid–liquid interface, and it is usual to adopt an averaged, continuum description of the resulting reactive, two-phase medium, called a mushy layer. Dependent variables of a mushy layer are the mean temperature, the mean interstitial salinity, and the mean volume fraction of the solid phase, with averages taken over a scale larger than the pore scale. Because the salt rejected by the solid phase can be accommodated within the interstices of a mushy layer, transport of salt is no longer a rate-limiting factor and the macroscopic envelopes of mushy layers are determined principally by heat transfer (Huppert and Worster 1985).

However, gradients of the interstitial salinity can drive convection in the interior of a mushy layer, and this is the dominant mechanism by which salt is delivered to the ocean during formation of sea ice: the salt flux from sea ice to ocean would be negligible in the absence of buoyancy forces, a fact that is insufficiently recognized in the parameterizations used in most current climate models.

The key ideas can be gleaned from the following simplified model. The equations governing an ideal mushy layer (Worster 1997) can be written as

$$\rho c_p\left(\frac{\partial T}{\partial t} + \mathbf{u}\cdot\nabla T\right) = k\nabla^2 T + \rho L\frac{\partial \phi}{\partial t},$$

$$(1-\phi)\frac{\partial S}{\partial t} + \mathbf{u}\cdot\nabla S = S\frac{\partial \phi}{\partial t},$$

$$\mu\mathbf{u} = \Pi(-\nabla p + \rho g),$$

together with the liquidus constraint and the continuity equation $\nabla \cdot \mathbf{u} = 0$. An approximate dimensionless form, when $\mathcal{S} \gg 1$, $\mathcal{C} \gg 1$ with $\mathcal{S}/\mathcal{C} = O(1)$, can be written as

$$\Omega \frac{D\theta}{Dt} = \nabla^2 \theta,$$
$$\mathbf{u} = R_m(-\nabla p + \theta k),$$
$$\frac{\partial \phi}{\partial t} = -\mathcal{C}^{-1} \frac{D\theta}{Dt},$$

where $\theta = [T - T_B]/[T_L(S_0) - T_B] = [S - S_L(T_B)]/[S_0 - S_L(T_B)]$ and $D/Dt \equiv \partial/\partial t + \mathbf{u} \cdot \nabla$ is the material derivative following the Darcy flow. Note that the first two equations are de-coupled from the third, which determines the evolution of the solid fraction in terms of the redistribution of solute. In particular, the third equation shows that there is dissolution ($\partial\phi/\partial t < 0$) whenever there is flow from cooler to warmer regions within a mushy layer. This is the cause of the brine channels that form in sea ice, for example.

The first two equations admit a steady solution with a linear vertical temperature gradient and no flow in an infinite horizontal layer, as depicted in Figure 35.5a. Perturbations to this solution can be analyzed by considering the normal modes

$$\theta = 1 - z + \hat{\theta}(z) e^{i\alpha x + \sigma t},$$
$$\omega = \hat{\omega}(z) e^{i\alpha x + \sigma t},$$

where ω is the vertical component of the velocity field. If these expressions are substituted into the governing equations and the resulting equations are linearized in the perturbation quantities, we obtain

$$-\Omega \hat{\omega} = (D^2 - \alpha^2)\hat{\theta},$$
$$(D^2 - \alpha^2)\hat{\omega} = \alpha^2 Ra_m \hat{\theta},$$

which can be combined to give

$$(D^2 - \alpha^2)^2 \hat{\omega} = -\alpha^2 \Omega Ra_m \hat{\omega}.$$

For illustration, we solve this perturbation equation subject to boundary conditions that the upper surface is impermeable and at constant temperature, so that

$$\hat{\omega} = 0, \quad \hat{\theta} = 0 \Rightarrow D^2 \hat{\omega} = 0 \quad (z = 0)$$

and that the lower boundary is held at constant pressure and heat flux, as is appropriate at a mush–liquid interface, so that

$$D\hat{\omega} = 0, \quad D\hat{\theta} = 0 \Rightarrow D^3 \hat{\omega} = 0 \quad (z = 1).$$

The eigenfunctions of this system are

$$\hat{\omega}_n = \sin\left[\left(n + \frac{1}{2}\right)\pi(1 - z)\right],$$

with corresponding eigenvalues

$$\Omega Ra_m = \frac{\left[\left(n + \frac{1}{2}\right)^2 \pi^2 + \alpha^2\right]^2}{\alpha^2}.$$

The most unstable mode has $n = 0$ and

$$\Omega Ra_m = \frac{(\pi^2/4 + \alpha^2)^2}{\alpha^2}.$$

This neutral curve has a minimum value of $\Omega Ra_m = \pi^2$ at $\alpha = \pi/2$. As a rule of thumb, a mushy layer growing from a region of melt will begin to convect when its modified Rayleigh number ΩRa_m exceeds a value of about 10 (Worster 1992).

35.3.4 Numerical Analysis

Numerical studies of phase change have employed a range of algorithms and different approaches. When phase boundaries are involved, a choice has to be made whether to "fit" the boundaries or to "capture" them. In the former case, separate computational domains are established for the solid and the liquid or the mush and the liquid, for example, and conditions are employed to relate variables across the interface between the domains as

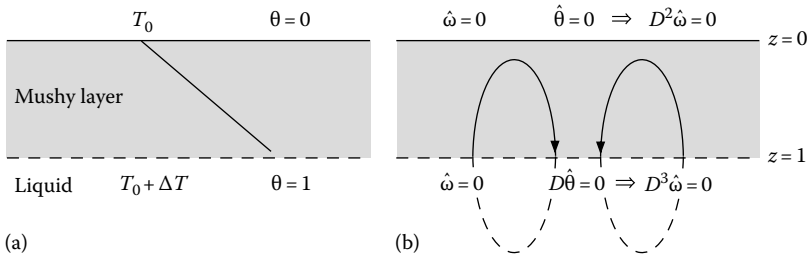

FIGURE 35.5 (a) A quiescent mushy layer above a deep liquid region with a linear temperature gradient imposed across it. (b) Small perturbations can lead to convective rolls, shown by the stream lines. Boundary conditions for the perturbed fields are shown.

well as to evolve the location of the interface. For solidification of a pure melt, for example, the diffusion equation would be applied to the solid domain, the Navier–Stokes equations and the advection–diffusion equation would be applied to the liquid domain, and an equilibrium constraint $T = T_m$ plus the Stefan condition could be applied at the solid–liquid interface. This mimics the approach usually taken in analytical studies, such as those described earlier.

Alternatively, equations are sought that apply, at least approximately, throughout the system, and the interface is subsequently located as a contour of one of the dependent variables. In the case of a pure melt of temperature $T_\infty > T_m$ brought into contact with a boundary of temperature $T_0 < T_m$, for example, the *enthalpy method* would start with uniform enthalpy $H(x, t = 0) = c_{ps}(T_\infty - T_m)$ throughout a fixed domain then, at each point, evolve the enthalpy according to

$$\frac{\partial H}{\partial t} = \frac{\partial}{\partial x}\left[k(\varphi)\frac{\partial T}{\partial x}\right],$$

where $k(\phi)$ is the conductivity, with the temperature T and the phase fraction ϕ determined by inverting

$$\begin{aligned} H &= c_{ps}(T - T_m), && \phi = 0 \quad \text{if} && H > 0, \\ H &= -\rho L\phi, && T = T_m \quad \text{if} && -\rho L < H < 0, \\ H &= c_{pl}(T - T_m) - \rho L, && \phi = 1 \quad \text{if} && H < -\rho L. \end{aligned}$$

Note that the phase fraction ϕ is an artifact of the method, related to the fact that the phase boundary would like to be between the fixed grid points of the numerical scheme and is not the same as the solid fraction ϕ of a mushy layer. Such methods can smear the solid–liquid interface over several grid points. The location of the phase boundary is usually identified with the contour $\phi = 0.5$. There are some drawbacks to such methods, but they can be outweighed by the convenience of computing on a single domain, particularly in higher dimensions if the phase boundary becomes convoluted.

Another single-domain approach is the *phase-field method*, which starts with a weak form of the governing equations and includes a gradient energy proportional to $|\nabla\phi|^2$, which leads to behavior that mimics the curvature undercooling associated with the Gibbs–Thomson effect. This method has been used extensively to study branched or dendritic growth of single crystals, including cases in which fluid flow is important (Boettinger et al. 2002).

An additional complication in using a single domain to compute solidification of systems involving mushy regions is the need for a single momentum equation that reduces to the Navier–Stokes equation in fully liquid regions and reduces to (or at least approximates) Darcy's equation in the interior of mushy regions. The most common choice is to use the Brinkmann equation, which adds Darcy friction to the Navier–Stokes equations with a permeability that tends to infinity as the solid fraction tends to zero. The two-domain approach for such problems has its own difficulties. Principally, because of the hyperbolic character of the differential operator acting on the solid fraction in the mushy layer equations, the treatment of mush–liquid interfaces depends crucially on whether the material flow is from liquid to mush or vice versa, which may not be known in advance of a computational time step.

As with all computational endeavors, there are horses for courses, and it pays to consider carefully the likely behavior of a system before choosing an appropriate algorithm.

35.3.5 Experimental Studies

Many solidifying systems of interest are opaque and have melting temperatures that are difficult or inconvenient for laboratory study. There have been significant advances in our understanding of the solidification of mixtures, in particular, made by studying the crystallization of aqueous salt solutions (Huppert 1990). Many of these are transparent, which has made possible visual observations of crystal habit and of convective flows in the melt. Flow observations have been made quite simply using dye streaks, shadowgraph images, or schlieren. These have revealed many fascinating phenomena, including double-diffusive convection of the melt (Figure 35.6) and plumes of residual fluid emanating from chimneys (called "brine channels" in the context of sea ice) formed by convection in mushy layers (Figure 35.7).

Temperature and composition (salinity) in solidifying systems can be measured using standard techniques: thermocouples or thermistors for temperature and conductivity probes or refractometers for concentration. More difficult to measure is the solid-fraction distribution in mushy regions. Probably the first direct measurement of solid fraction was made using X-ray tomography in a medical facility after completion of an experiment (Chen 1995). More recently, magnetic resonance imaging (MRI)

FIGURE 35.6 **(See color insert.)** A vertical block of ice melting into a warm, stratified salt solution. Double-diffusive convection results in the formation of nearly horizontal, nearly uniform layers of water that are colder and fresher than the environment.

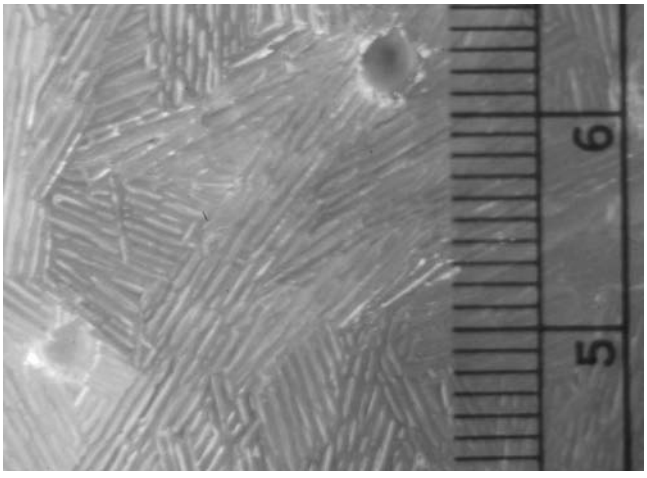

(a)

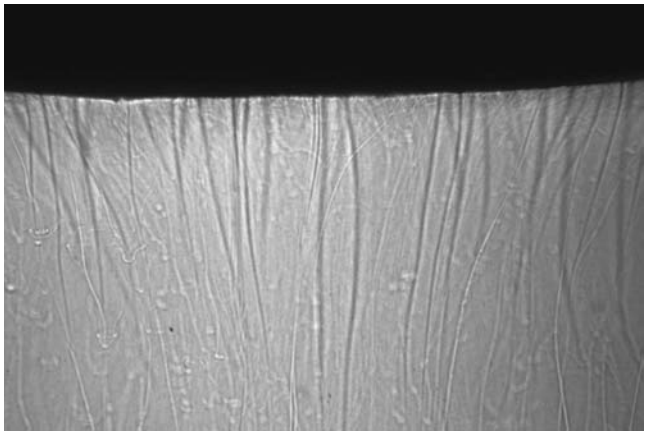

(b)

FIGURE 35.7 (See color insert.) (a) The underside of columnar sea ice, showing ice platelets spaced slightly less than a millimeter apart and two brine channels of approximately 3 mm diameter. (b) A shadowgraph image of the side view of growing sea ice (the black region at the top), showing the plumes of dense brine that emanate from brine channels and deliver salt to the underlying ocean. The image is of a region approximately 20 cm wide.

has been used under laboratory conditions to measure the evolution of solid fraction as well as the internal structure of chimneys (Aussillous et al. 2006). MRI has also been used in field experiments, exploiting the Earth's magnetic field to measure the brine diffusivity and volume fraction of ice in thick multiyear sea ice with a vertical resolution of about 20 cm (Callaghan et al. 1999). The evolution of solid fraction in growing sea ice has been measured in situ with a vertical resolution of 1 cm by measuring the electrical impedance between pairs of horizontal wires around which the ice grew (Notz et al. 2005). Such nondestructive techniques as MRI or electrical impedance methods are important to develop if accurate remote monitoring of sea ice is to be achieved.

To this end, there is considerable effort in developing ways to sense the state of sea ice from orbiting satellites. Some variables, such as ice extent and ice concentration (area fraction covered by ice), are relatively straightforward to detect by electromagnetic methods. On the other hand, ice thickness is very difficult to determine, in part because of snow and in part because the reflectivity to the microwaves used depends on the electrical properties of sea ice, which are sensitive to its brine content. Currently, more accurate measurements of ice thickness are made using upward-looking sonar from submarines, but such data is sparse compared to the coverage that could in principle be obtained by satellite (Kwok and Rothrock 2009).

35.4 Applications

As indicated in the Introduction, there is a vast range of applications involving fluid flow coupled with phase change. Here we sketch a few interesting examples.

The inner core of the Earth, of current radius 1221 km, representing 0.5% by volume and 2% by mass of the Earth, grows slowly by deposition of almost pure iron from the fluid outer core of molten iron and roughly 10% of impurities such as oxygen, sulfur, and nickel. The deposition rate is 2×10^6 kg s^{-1}, approximately two orders of magnitude larger than the total iron and steel production on the surface of the Earth, yet the radius of the inner core currently increases at only about 1 mm per year. The compositional convection driven by the relatively light fluid (enriched in impurities) released during solidification through an electrically conducting medium maintains the magnetic field of the Earth. Without this field, life would be impossible because the field deflects the solar wind that would otherwise blow away the atmosphere. The inner core was initiated approximately 2×10^9 years ago and will become completely solidified after another 2×10^{10} years (by which time the sun will have burned itself out). The growth of the inner core is currently controlled by a balance between the decrease in heat content of the cooling outer core and the heat flux out at the top because the effective Stefan number is relatively small.

Solidification plays an essential role in igneous petrology—the study of rocks derived from a liquid melt of volcanic origin. The rich multicomponent melts solidify in magma chambers (large storage reservoirs of partially molten rock that power volcanic eruptions), in volcanic conduits, and in lava flows. An important component, even though present in small amounts (of order 1% by weight) is dissolved gas (such as H_2O and CO_2) which can exsolve due to pressure release and temperature change and alter the form of the resulting solid as well as drive vigorous motion. This is an area of extreme laboratory investigations, using very high temperatures and pressures. An example of considerable financial importance is the rather exotic magma formed up to 450 km beneath the surface of the Earth that rises in so-called kimberlite pipes and is the major source of the world's diamonds (Sparks et al. 2009).

A vertical surface of ice surrounded by water stratified by salt melts to produce a layered structure, as shown in Figure 35.6. While the relatively fresh meltwater rises in a thin, turbulent boundary layer adjacent to the ice, cooling extends further into the liquid region and drives a downward flow that detrains into

the stratified exterior when it reaches a level of neutral buoyancy. Mixing between these counter-flowing layers increases the salinity of the rising meltwater and takes some of it into the horizontal layers, which thus ruins the potential to harvest freshwater simply from icebergs. The thickness of the intruding layers can be determined quantitatively; and the theory has been compared successfully against numerous laboratory experiments (Huppert and Turner 1981) and the layers formed adjacent to the Erebus Glacier Tongue in the Antarctic.

The solidification of multicomponent melts in molds is an essential and very successful aspect of the metallurgical industry (Hurle 1993). Amorphous (noncrystalline) alloys called glasses can be produced by spin casting at rapid cooling rates of millions of degrees per second. Glasses also occur as a result of rapid volcanic eruptions, both within volcanic conduits and in the resultant hot plume cooled by contact with the atmosphere. By contrast, epitaxy is a process of slow deposition of a thin film onto a monocrystalline substrate from either gaseous or liquid precursors. The substrate acts as a seed crystal and the epitaxial film adopts its crystalline structure and orientation. Epitaxy is widely used to manufacture silicon-based semiconductors such as bipolar junction transistors within integrated-circuit microcontrollers and microprocessors. At a more prosaic level, concrete solidifies on mixing and reacting with water to be the world's most used synthetic material, approximately 8 km^3 being manufactured each year (more than 1 m^3 per person per year) in a multibillion-dollar industry that contributes approximately 5% of the world's anthropogenic emission of CO_2.

Clathrate hydrates, first documented by Sir Humphrey Davy in 1810, consist of a molecular cage of solid ice enclosing gases such as water vapor, methane, carbon dioxide, and hydrogen sulfide (Buffett 2000). They form at high pressures, and on Earth they exist within sea-floor sediments along deep continental margins. In the Martian ice caps, they sequester large amounts of water vapor and carbon dioxide from the atmosphere. It has been estimated that on Earth about 10^{12} kg of carbon is trapped in oceanic sediments as methane hydrates with a smaller amount in permafrost regions, a total that represents the largest hydrocarbon source on Earth. Because methane is such a strong greenhouse gas, the release of large quantities of methane from these hydrates could have serious consequences for global climate.

Intermolecular disjoining forces exist between ice and many other materials when they are brought into contact. These cause the ice to melt (*pre-melt* because this phenomenon occurs at temperatures below the bulk melting temperature) in a thin surface film (of the order of tens of nanometers) and generate high pressures between the ice and its substrate that cause water to be sucked toward colder regions of partially frozen, saturated soils (Wettlaufer and Worster 2006). This is the underlying cause of frost heave, which results in potholes in roads and is a major geomorphological agent, fracturing rocks and forming various types of patterned ground.

Significant attention is currently being paid to the fate of sea ice, which may soon be absent from the Arctic Ocean during summer months, though the ocean is likely to remain ice-covered in winter for the foreseeable future. The seasonal waxing and waning of the sea-ice cover drives a high-latitude distillation process in the oceans: salt is rejected by the growing sea ice and is carried buoyantly into the mixed layer or deeper into the abyss; melting sea ice forms a relatively fresh cap on the oceans that resists convective overturning. After the initial buoyancy-driven instability described earlier, brine convecting in the interstices of sea ice dissolves the ice matrix to form channels that provide the principal conduit for salty plumes to be injected into the ocean (Figure 35.7, Wettlaufer et al. 1997).

On the surface of very young sea ice, when it is only a few centimeters thick, beautiful fern-like clusters of ice crystals called frost flowers can form. Concentrated brine is wicked up from the interstices of the underlying sea ice to form a liquid surface layer on frost flowers in which bromides from seawater are converted to bromine monoxide, which is carried into the atmosphere and contributes to the depletion of ozone. High in the atmosphere, the pre-melted surfaces of ice crystals enhance a wide range of reactions, making ice a key component of atmospheric chemistry.

35.5 Major Challenges

Interactions between phase change and fluid flow involve physics on a vast range of scales, from the nanoscale of pre-melted liquid films through the microscale of dendritic snowflakes and the interstices of mushy layers, to the macroscales of brine channels and the megascales of ocean circulations. The major challenges facing this branch of science relate to understanding the physics of these multiscale processes sufficiently to codify them efficiently within predictive mathematical models. There are important questions relating to the evolution of sea ice and the associated brine fluxes that contribute significantly to the thermohaline circulation driving, together with wind stresses, the Gulf Stream, and other major oceanic features that affect regional climate.

The mathematics of phase change is relevant to other systems that do not involve thermodynamic phase change. Examples include predicting the shape and evolution of alluvial fans, where the advancing phase is the sedimentary bed; calculating the heat and salt fluxes across double-diffusive interfaces, where the phases are turbulent and quiescent fluid regions; and establishing the location and stability of marine-ice-sheet grounding lines, separating grounded ice sheets from floating ice shelves. In all these examples, the major challenge is to understand the physical processes sufficiently to derive tractable mathematical models capable of making robust predictions.

It is clear that flows involving phase change are an integral part of many phenomena and processes that affect our environment. Their understanding requires collaborations across many scientific disciplines, and it is essential that the mathematical and numerical approaches that are increasingly used to make predictions of our future environment are tested against well controlled and characterized experiments.

Acknowledgments

We are grateful to Jerome Neufeld, Dominic Vella, and John Wettlaufer for their helpful comments on a draft of the manuscript. Herbert E. Huppert is supported by a Royal Society Wolfson Merit Award, for which he is grateful.

References

Aussillous, P., Sederman, A.J., Gladden, L.F., Huppert, H.E., and Worster, M.G. 2006. Magnetic resonance imaging of structure and convection in solidifying mushy layers. *J. Fluid Mech*. **552**, 99–125.

Boettinger, W.J., Warren, J.A., Beckermann, C., and Karma, A. 2002. Phase-field simulation of solidification. *Annu. Rev. Mater. Res*. **32**, 163–194.

Buffett, B.A. 2000. Clathrate hydrates. *Annu. Rev. Earth Planet. Sci*. **28**, 477507.

Callaghan, P.T., Dykstraa, R., Ecclesa, C.D., Haskellb, T.G., and Seymour, J.D. 1999. A nuclear magnetic resonance study of Antarctic sea ice brine diffusivity. *Cold Reg. Sci. Technol*. **29**(2), 53–171.

Carslaw, H.S. and Jaeger, J.C. 1959. *Conduction of Heat in Solids*. Oxford University Press, Oxford, U.K.

Chen, C.F. 1995. Experimental study of convection in a mushy layer during directional solidification. *J. Fluid Mech*. **293**, 81–98.

Davis, S.H. 2001. *Theory of Solidification*. Cambridge University Press, Cambridge, U.K.

Gill, A.E. 1982. *Atmosphere–Ocean Dynamics*. International Geophysics Series, Vol. 30. Academic Press, New York.

Huppert, H.E. 1990. The fluid mechanics of solidification. *J. Fluid Mech*. **212**, 209–240.

Huppert, H.E. and Turner, J.S.T. 1981. Double-diffusive convection. *J. Fluid Mech*. **106**, 299–329.

Huppert, H.E. and Worster, M.G. 1985. Dynamic solidification of a binary melt. *Nature* **314**, 703–707.

Hurle, D.T.J. (ed.) 1993. *Handbook of Crystal Growth*. Elsevier, Amsterdam, the Netherlands.

Kwok, R. and Rothrock, D.A. 2009. Decline in Arctic sea ice thickness from submarine and ICESat records: 19582008. *Geophys. Res. Lett*. **36**, L15501.

Notz, D., Wettlaufer, J.S., and Worster, M.G. 2005. A non-destructive method for measuring salinity and solid fraction of growing sea ice in situ. *J. Glac*. **51**(172), 159–166.

Sparks, R.S.J., Brooker, R.A., Field, M., Kavanagh, J., Schumacher, J.C., and Walter, M.J. 2009. The nature of erupting kimberlite melts. *Lithos* **112**, 429–438.

Stevens, B. 2005. Atmospheric moist convection. *Annu. Rev. Earth Planet. Sci*. **33**, 605–643.

Turner, J.S. 1979. *Buoyancy Effects in Fluids*. Cambridge University Press, Cambridge, U.K.

Wettlaufer, J.S. and Worster, M.G. 2006. Premelting dynamics. *Annu. Rev. Fluid Mech*. **38**, 427–452.

Wettlaufer, J.S., Worster, M.G., and Huppert, H.E. 1997. Natural convection during solidification of an alloy from above with application to the evolution of sea ice *J. Fluid Mech*. **344**, 291–316.

Worster, M.G. 1992. Instabilities of the liquid and mushy regions during solidification of alloys. *J. Fluid Mech*. **237**, 649–669.

Worster, M.G. 1997. Convection in mushy layers. *Annu. Rev. Fluid Mech*. **29**, 91–122.

Worster, M.G. 2000. Solidification of fluids. In *Perspectives in Fluid Dynamics*, eds. G.K. Batchelor, H.K. Moffatt, and M.G. Worster, pp. 393–496. Cambridge University Press, Cambridge, U.K.